Analysis of DC and AC Choke Effects on Common-Mode Noise Emissions in ASD at the Frequency Range of 9–150 kHz

Ganjavi, Amir; Rathnayake, Hansika; Kumar, Dinesh; Zare, Firuz; Abbosh, Amin; Davari, Pooya

Published in:
2020 IEEE International Conference on Power Electronics, Drives, and Energy Systems (PEDES 2020)

DOI (link to publication from Publisher):
10.1109/PEDES49360.2020.9379827

Publication date:
2020

Document Version
Accepted author manuscript, peer reviewed version

Analysis of DC and AC Choke Effects on Common-Mode Noise Emissions in ASD at the Frequency Range of 9–150 kHz

1st Amir Ganjavi
School of ITEE
The University of Queensland
Brisbane, Australia
a.ganjavi@uq.net.au

2nd Hansika Rathnayake
School of ITEE
The University of Queensland
Brisbane, Australia
h.rathnayake@uq.edu.au

3rd Dinesh Kumar
Global Research and Development Center
Danfoss Drives A/S
Gråsten, Denmark
dineshr30@ieee.org

4th Firuz Zare
School of ITEE
The University of Queensland
Brisbane, Australia
f.zare@uq.edu.au

5th Amin Abbosh
School of ITEE
The University of Queensland
Brisbane, Australia
a.abbosh@uq.edu.au

6th Pooya Davari
Department of Energy Technology
Aalborg University
Aalborg, Denmark
pda@et.aau.dk

***Abstract*—Magnetic chokes are conventionally utilized at the DC or AC side of the Adjustable Speed Drives (ASDs) to suppress low order harmonics of 0–2 kHz. Recently, the frequency range of 9–150 kHz has been noticed as a new disturbing frequency range, interfering with the distribution networks. Due to the novelty of this topic, so far, there has not been a thorough investigation for the effect of DC and AC choke configurations on 9–150 kHz emissions, especially for the three-phase ASDs. In this paper, the effect of DC and AC choke configurations on Common-Mode (CM) current emissions at the frequency range of 9–150 kHz is broadly surveyed in the three-phase ASDs. Subsequently, the comprehensive equivalent models of the system are presented for each configuration of DC and AC chokes. This investigation is based on the comparative analysis of the system's transfer functions according to the presented single-phase equivalent model, mathematical calculations, and the three-phase system circuit. Consequently, the presented approach is highly useful to minimize the drive system volume, as the designer can predict the choke configuration of the smallest size for suppressing 9–150 kHz emissions.**

***Index Terms*—Common-Mode noise, filter design, three-phase adjustable speed drive, 9-150 kHz.**

I. Introduction

Nowadays, a great deal of the world's energy is harvested through Adjustable Speed Drives (ASDs) [1]–[3]. Subsequently, according to Fig. 1, more than 40% of the global energy is consumed by the electric-motor driven systems [4]. Until now, drive manufacturers should meet the the Electromagnetic Compatibility (EMC) requirements for the frequency ranges of 0–2 kHz and 0.15–30 MHz [5]. Recently, due to the significant advances in power electronics technology, there is a growing tendency to increase the switching frequency of electronic devices in order to improve the operation and reduce the total size of the system. In fact, the switching frequency of these devices typically takes place at the range of 2–150 kHz. Accordingly, the characteristic of emissions has been changed in terms of magnitude and frequency range [6]–[11]. As a result, the frequency range of 2–150 kHz is recognized as a new frequency range, interfering with the distribution networks [12]–[14]. This frequency range is divided into 2–9 kHz and 9–150 kHz ranges according to the IEC (International Electrotechnical Commission) Sub-Technical Committee 77A (SC77A). Consequently, due to the importance of this new frequency range, the drive manufactures are taking serious steps to design filters for this range in order to devise for the emerging EMC standards of the 2–150 kHz [15].

Electromagnetic Interference (EMI) is divided into two types: 1- Differential-Mode (DM) currents 2- Common-Mode (CM) currents. Separating these two emissions is of great importance to design the DM and CM filters, meeting the standard requirements. Although many studies have been conducted to separate these two emissions for the single-phase drive systems, there are very limited investigations for the three-phase ASDs. These investigations even get narrower for the emerging range of 2–150 kHz. Recently, a limited number of investigations have been carried out for analyzing the factors affecting the filter design at the new frequency range of 2-150 kHz.

In [15], an improved asymmetrical model of AC machine compatible with the emerging 2–150 kHz standard has been proposed. Moreover, an approach has been suggested to model different sub-systems in the three-phase ASD. Accordingly, the presented model can be useful for simulation-based filter

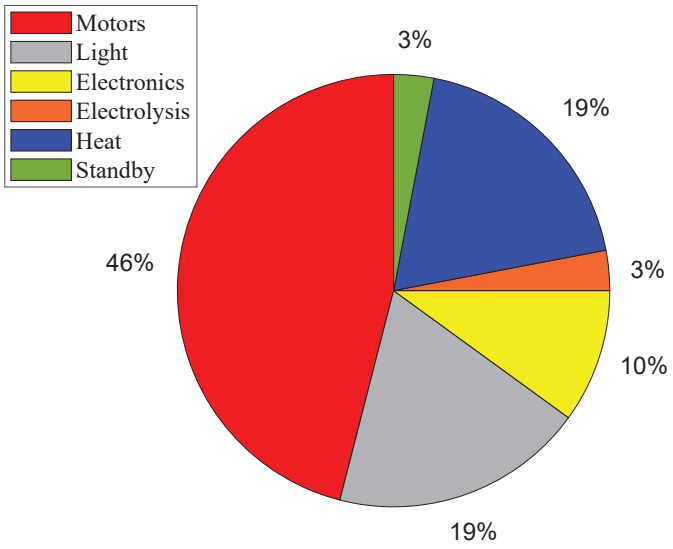

Fig. 1. Estimated allocation of worldwide electricity demand by end-use [4].

design at the frequency range of 2–150 kHz through prediction of resonances in the system.

In [16], factors affecting the filter design in the three-phase ASDs have been investigated for 0–2 kHz and the new frequency range of 2–9 kHz. Accordingly, effects of DC-link filter, cables, and EMI filter (including CM capacitors and inductors) have been analyzed by presenting a system model. In [17], an estimation method has been proposed to predict resonances in the three-phase ASDs for the frequency range of 9-150 kHz. In fact, the estimation approach is based on the impedance analysis of the CM equivalent circuit model for the three-phase ASD. Consequently, the CM noise circulations in the drive system can be analyzed for the EMI filter design at the new frequency range of 9-150 kHz.

Fig. 2 shows the typical configuration of a three-phase ASD. According to Fig. 2, in order to comply with the standard related to the low frequency range of 0–2 kHz, chokes are placed at the DC or AC side of the system, known as DC and AC chokes, respectively. Although theses chokes are conventionally aimed at suppressing the low frequency harmonics of 0–2 kHz, their configurations can affect emissions in the emerging frequency range of 2–150 kHz. Until now however, as far as our knowledge goes, there has not been a clear investigation for the effect of choke configurations on the EMI emissions.

In this paper, effects of DC and AC choke configurations on the CM emissions in the frequency range of 9–150 kHz are investigated. Accordingly, the CM equivalent circuits of the three-phase drive system, including DC and AC chokes, are presented. In this study, an approach is proposed to predict the attenuation/amplification range of the CM current from the motor to Line Stabilization Network (LISN), based on the transfer functions of the equivalent CM circuit. As a result, the proposed strategy gives the designer useful information on the most effective choke configuration to suppress the emissions of 9–150 kHz.

II. CM Equivalent Circuit Model

According to Fig. 2, there are four main CM loops in the system: 1- CM current flowing through the motor ($i_{g-Motor}$) 2- CM current flowing through the DC-Link filter ($i_{g-DCLink}$) 3- CM current flowing through the EMI filter (i_{g-EMI}), and 4- CM current flowing through the LISN (i_{LISN}). In order to analyze the effect of DC and AC choke configurations on emissions of 9–150 kHz range, the Laplace transfer functions of the CM loops ($i_{g-DCLink}/i_{g-Motor}$, $i_{g-EMI}/i_{g-Motor}$, and $i_{LISN}/i_{g-Motor}$) are extracted. In fact, the main duty of the filters is to reduce the magnitude of the transfer function $i_{LISN}/i_{g-Motor}$ although analysis of $i_{g-DCLink}/i_{g-Motor}$ and $i_{g-EMI}/i_{g-Motor}$ is also useful for designing the filters. Therefore, by defining these transfer functions, it can be predicted how $i_{g-Motor}$ is amplified or attenuated at the grid side based on configurations of DC or AC chokes.

The aforementioned transfer functions of the system will be extracted based on the single-phase CM equivalent circuit of the drive with configurations of DC and AC chokes. Subsequently, Fig. 3 shows the presented CM equivalent circuit when the DC or AC chokes are assigned in the drive system. It is to be noted that the equivalent circuit is extracted under the assumption that the drive system is symmetrical and balanced. In this equivalent model, the parasitic elements of the EMI filter, chokes and AC machines are extracted through the experimental measurements [15]. This is due to the fact that these parasitic elements are critically important when analyzing the CM emissions. Subsequently, Table I describes the parameters and specifications of the investigated drive system.

Fig. 4 shows the current route in ASD at a specific commutation interval of rectifier diodes. According to Fig. 4 (a), at each commutation interval of diodes, DC chokes add the impedance of 2×L_{dc} to the CM loop. On the other hand, according to Fig. 4 (b), AC chokes add the impedance of 2×L_{ac} to the CM loop at each commutation interval of rectifier diodes. Therefore, in order to draw a fair comparison, the inductance values assigned for each DC choke (L_{dc}) and AC choke (L_{ac}) are 1.25 mH; thus, at each commutation interval of the system, a circuit loop is created containing the impedance of 2×1.25 mH for both DC and AC choke configurations.

According to Fig. 3, the CM voltage (i.e., v_{CM} as shown in Fig. 2) is generated by two sources: 1- Grid side voltage through the diode rectifier, which is the low-frequency CM voltage (v_{CM-LF}), and 2- Pulse-Width Modulation (PWM) output voltage through the inverter, which is the high-frequency CM voltage (v_{CM-HF}). In this paper, the authors have modeled the CM voltage based on the high frequency PWM signals (v_{CM-HF}). Then the simulated transfer functions of the presented model along with the mathematical equations are provided to evaluate the procedure. It is to be noted that according to Fig. 3, the LISN utilized in the system is based on the CISPR16 for analysis of the 9–150 kHz range.

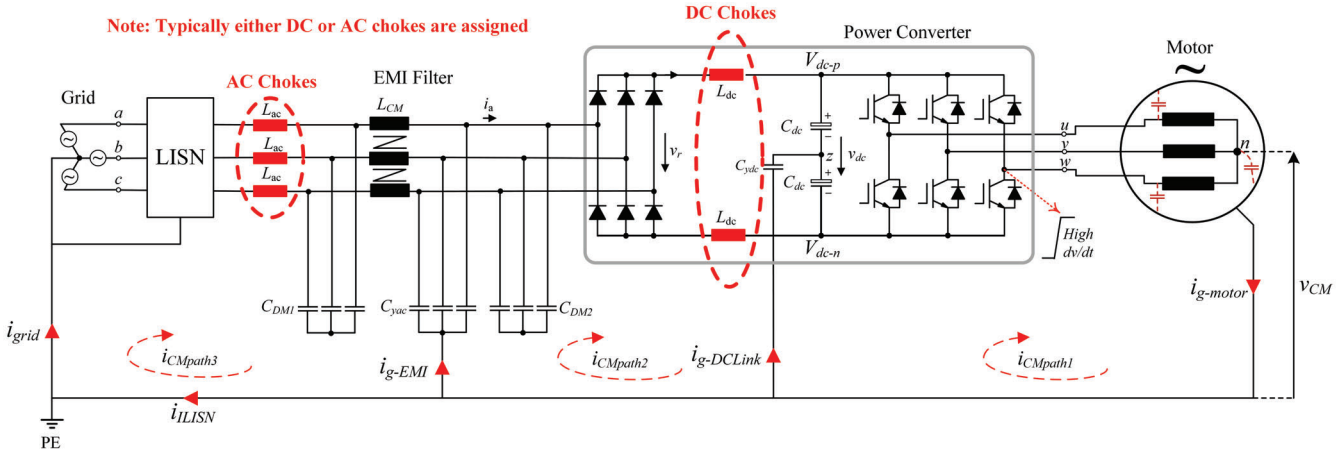

Fig. 2. Typical motor drive system, excluding motor cables.

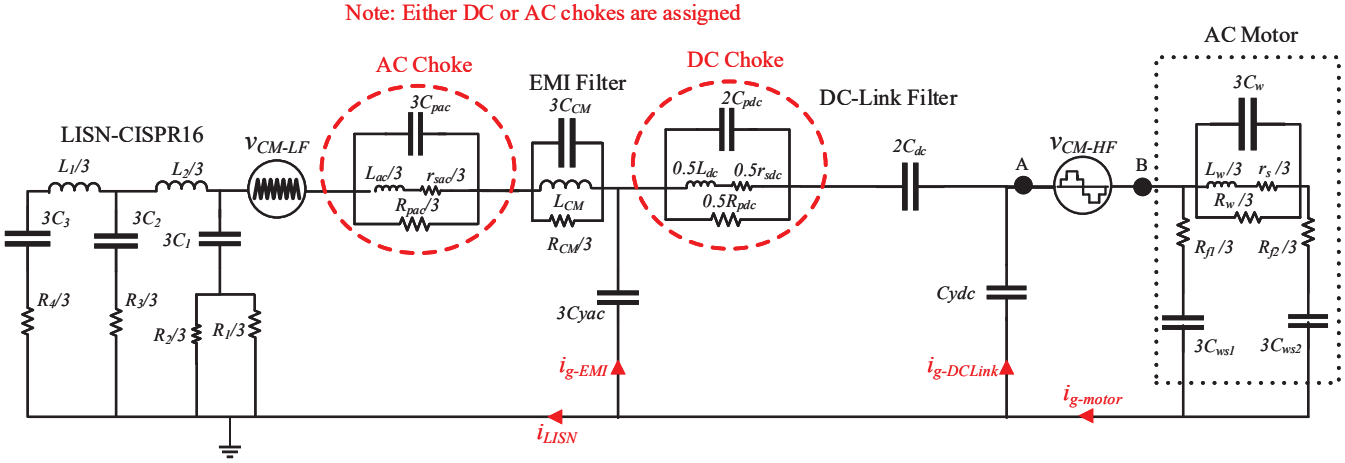

Fig. 3. CM equivalent circuit of the drive system when either AC or DC chokes are assigned in the system.

TABLE I
SPECIFICATIONS OF THE DRIVE SYSTEM

Parameters	L_{dc}, C_{dc}, r_{sdc}, R_{pdc}, C_{pdc}	L_{ac}, r_{sac}, R_{pac}, C_{pac}	L_w, C_w, C_{ws1}, C_{ws2}, r_s, R_w, R_{f1}, R_{f2}	Switching Frequency	Rated Power
Value	1.25 mH, 1000 μF, 0.28 Ω, 1.29 kΩ, 228 pF	1.25 mH, 0.28 Ω, 1.29 kΩ, 228 pF	9.4 mH,4.6 pF, 680 pF, 1100 pF, 9.5 Ω, 12.7 kΩ, 20 Ω, 13 Ω	5 kHz	7.5 kW

III. COMPARATIVE STUDY

In this section, the ability of DC and AC choke configurations in suppressing emissions at 9-150 kHz is compared. This comparison is based on the the transfer functions of CM equivalent circuit (see Fig. 3). According to the discussion in the previous section, in order to have a fair comparison, DC and AC choke volumes are chosen to get the same performance in terms of current Total Harmonic Distortion (THD).

A. ASD with DC Choke Configuration

In order to extract the transfer functions of the presented model in, v_{CM-HF} has been analyzed in the ANSYS Simplorer software to model the CM voltage created by the PWM inverter. To validate the transfer functions extracted by ANSYS software, the mathematical calculations of these transfer functions with constant coefficients have been extracted as (1)–(3). Also, the constant coefficients of (1)–(3) are provided in the Appendix. Consequently, Fig. 5 shows the comparison between the modeled transfer functions through ANSYS Simplorer software and the mathematically calculated ones. According to Fig. 5, the model and calculations accurately match with each other, validating the extracted model in the software.

$$\frac{i_{g-DCLink}(s)}{i_{g-Motor}(s)} = \frac{\sum_{i=0}^{9} a_i s^i}{\sum_{i=0}^{9} m_i s^i} \tag{1}$$

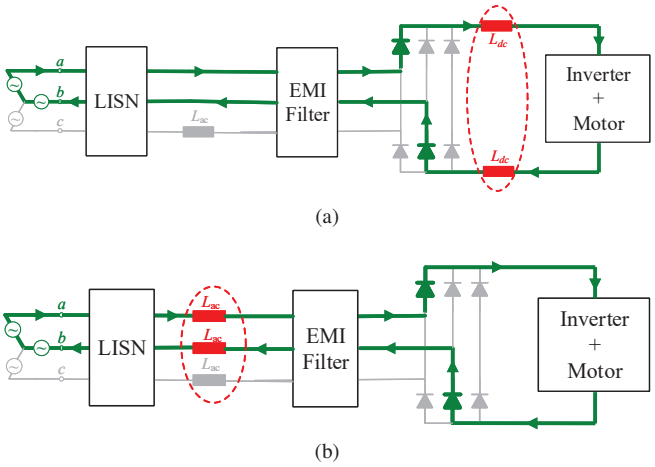

Fig. 4. Current route in ASD at a commutation interval of rectifier diodes. (a) ASD with DC choke, (b) ASD with AC choke.

$$\frac{i_{g-EMI}(s)}{i_{g-Motor}(s)} = \frac{\sum_{i=0}^{9} b_i s^i}{\sum_{i=0}^{9} m_i s^i} \tag{2}$$

$$\frac{i_{LISN}(s)}{i_{g-Motor}(s)} = \frac{\sum_{i=0}^{8} c_i s^i}{\sum_{i=0}^{9} m_i s^i} \tag{3}$$

B. ASD with AC Choke Configuration

With the same scenario explained above, transfer functions of the system can be extracted when the AC chokes are assigned in the system. Subsequently, Fig. 6 shows the comparison between the modeled transfer functions of the system assigned with DC and AC chokes. According to Fig. 6 (c), at the frequencies less than 30 kHz, AC chokes provide better attenuation/damping of the CM current at the LISN side though at higher frequencies, DC chokes outperform in terms of CM current attenuation. This is a critically important factor in filter design for the emerging frequency range of 2–150 kHz, as the designer can choose the most optimum choke configurations to minimize the measured CM current flowing through the LISN.

To evaluate the ability of the presented single-phase models to predict the amplification/attenuation rate of $i_{g-Motor}$ at the LISN side, the Fast Fourier Transform (FFT) of the related currents in the real-case three-phase drive system (see Fig. 2) have been extracted as shown in Fig. 7, using MATLAB software. In fact, these plots are provided for both DC and AC choke configurations in the drive.

By comparing Figs. 5, 6 and 7, it can be noted that the extracted model can optimally predict the CM current behavior. According to Fig. 7 (c), it can be realized that at low frequencies (less than 30 kHz), harmonics at the LISN side are more effectively attenuated when the AC chokes are assigned in the system; however, at higher frequencies, the DC chokes prove to be more effective. These findings are fully in alliance with the predictive model in Fig. 6 (c). Moreover. According to Fig. 7 (c), it can be noted that if only DC chokes are applied

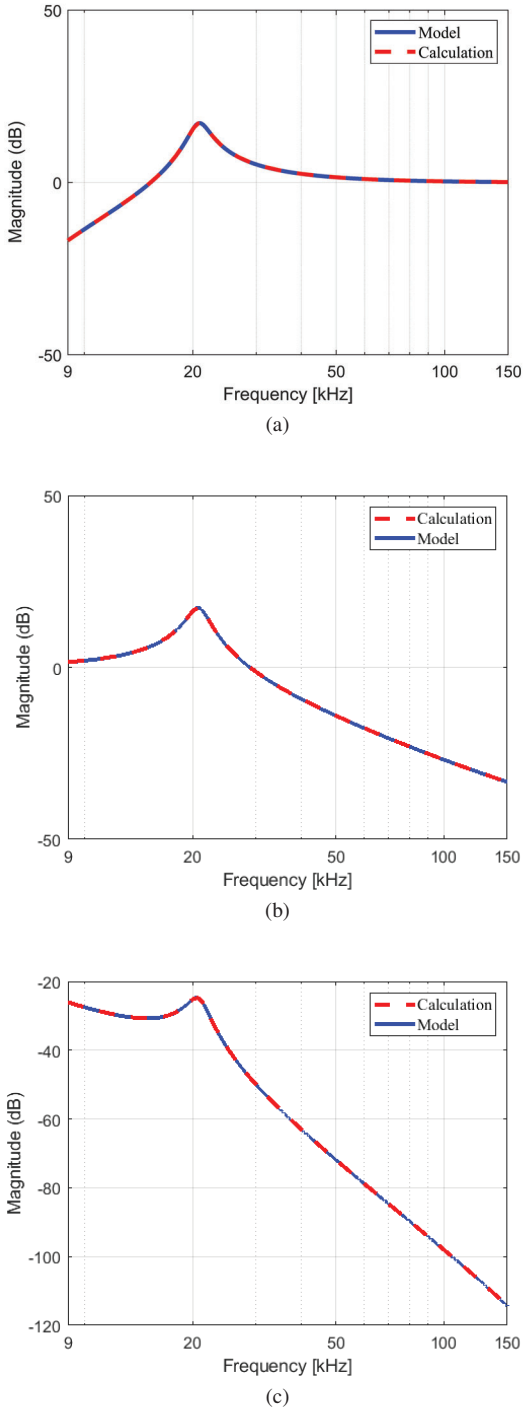

Fig. 5. Modeled (ANSYS) and calculated transfer functions of the system when DC chokes are assigned. (a) $\frac{i_{g-DCLink}(s)}{i_{g-Motor}(s)}$, (b) $\frac{i_{g-EMI}(s)}{i_{g-Motor}(s)}$, (c) $\frac{i_{LISN}(s)}{i_{g-Motor}(s)}$.

in the system, bigger CM chokes may be needed. This could be attributed to the fact that according Fig. 7 (c), when using only DC chokes in the system, the cut-off frequency of the CM filter should be at a lower frequency range as the amplitudes of the transfer function is higher at below 30 kHz compared

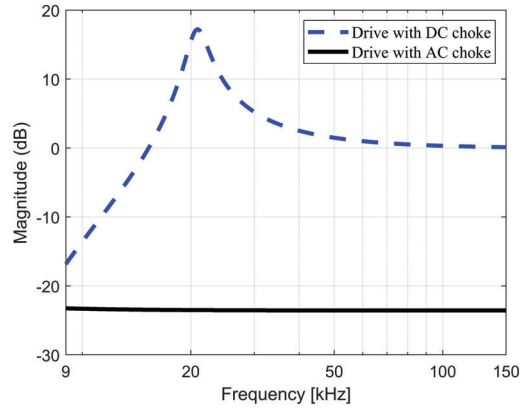

(a)

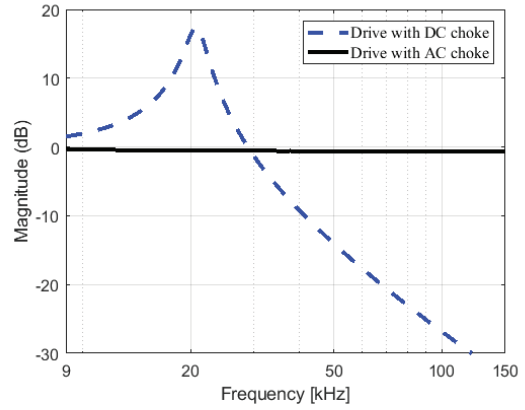

(b)

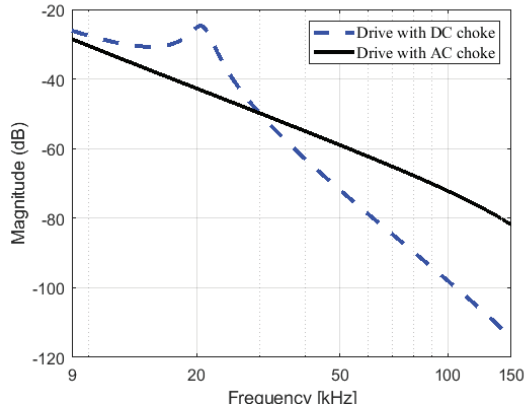

(c)

Fig. 6. Comparison between the modeled transfer functions of the system assigned with DC and AC chokes. (a) $\frac{i_{g-DCLink}(s)}{i_{g-Motor}(s)}$, (b) $\frac{i_{g-EMI}(s)}{i_{g-Motor}(s)}$, (c) $\frac{i_{LISN}(s)}{i_{g-Motor}(s)}$.

to when utilizing AC chokes in the system.

IV. Conclusion

In this paper, an approach was proposed to compare the capability of DC and AC chokes in suppressing emissions at the frequency range of 9-150 kHz. The presented method is based on calculation of the system transfer functions of the equivalent single-phase CM circuit. The results validate that the extracted transfer functions can predict the behavior of different choke configurations towards attenuation/amplification of $i_{g-Motor}$ at the LISN side of the three-phase ASD. Accordingly, in this case study, it is shown that at low frequencies (9-30 kHz), AC chokes could more effectively attenuate $i_{g-Motor}$, while DC chokes outperformed at higher frequencies (30-150 kHz). This approach is highly useful to optimize the size of the system, as the designer can achieve the choke configuration of the smallest volume leading to effectively suppressing the emissions.

Appendix
Transfer Function Coefficients [see (1)–(3)]

$$\frac{i_{g-DCLink}(s)}{i_{g-Motor}(s)}:$$

a_0=1.3230 $\times 10^{156}$, a_1=1.2888 $\times 10^{152}$, a_2=2.8991 $\times 10^{149}$, a_3=1.5391 $\times$ 10^{145},a_4=5.7998 $\times$ 10^{140}, a_5=1.4739 $\times$ 10^{136}, a_6=2.7040 $\times$ 10^{131}, a_7=2.0317 $\times$ 10^{126}, a_8=1.82 $\times$ 10^{120}, a_9=2.5411 $\times 10^{111}$.

m_0=4.9672 $\times$ 10^{158}, m_1=2.7333 $\times$ 10^{154}, m_2=4.5231 $\times$ 10^{150}, m_3=2.1280 $\times 10^{146}$, m_4=5.0183 $\times 10^{141}$, m_5=5.1377 $\times$ 10^{136}, m_6=3.3218 $\times 10^{131}$, m_7=2.0692 $\times 10^{126}$, m_8=1.8284 $\times$ 10^{120}, m_9=2.5527 $\times$ 10^{111}.

$$\frac{i_{g-EMI}(s)}{i_{g-Motor}(s)}:$$

b_0=1.8305 $\times 10^{157}$, b_1=1.7002 $\times 10^{153}$, b_2=3.6430 $\times 10^{150}$, b_3=1.9250 $\times$ 10^{146},b_4=4.4298 $\times$ 10^{141}, b_5=3.6631 $\times$ 10^{136}, b_6=6.1777 $\times$ 10^{130}, b_7=3.7499 $\times$ 10^{124}, b_8=8.3355 $\times$ 10^{117}, b_9=1.1584 $\times 10^{109}$.

$$\frac{i_{LISN}(s)}{i_{g-Motor}(s)}:$$

c_0=4.7709 $\times 10^{158}$, c_1=2.5504 $\times 10^{154}$, c_2=5.9016 $\times 10^{149}$, c_3=4.9053 $\times$ 10^{144},c_4=8.5799 $\times$ 10^{138}, c_5=7.3746 $\times$ 10^{132}, c_6=5.0120 $\times 10^{126}$, c_7=2.3474 $\times 10^{120}$, c_8=5.1758 $\times 10^{113}$.

Acknowledgment

The authors would like to thank the Australian Research Council, supporting FT150100042 and LP170100902 projects.

References

[1] Y. Li, H. Lin, H. Huang, C. Chen, and H. Yang, "Analysis and performance evaluation of an efficient power-fed permanent magnet adjustable speed drive," *IEEE Transactions on Industrial Electronics*, vol. 66, no. 1, pp. 784–794, 2019.

[2] U. Choi, S. Jørgensen, and F. Blaabjerg, "Impact of cooling system capacity on lifetime of power module in adjustable speed drives," *IEEE Journal of Emerging and Selected Topics in Power Electronics*, vol. 7, no. 3, pp. 1768–1776, 2019.

[3] P. Davari, Y. Yang, F. Zare, and F. Blaabjerg, "A multipulse pattern modulation scheme for harmonic mitigation in three-phase multimotor drives," *IEEE Journal of Emerging and Selected Topics in Power Electronics*, vol. 4, no. 1, pp. 174–185, 2016.

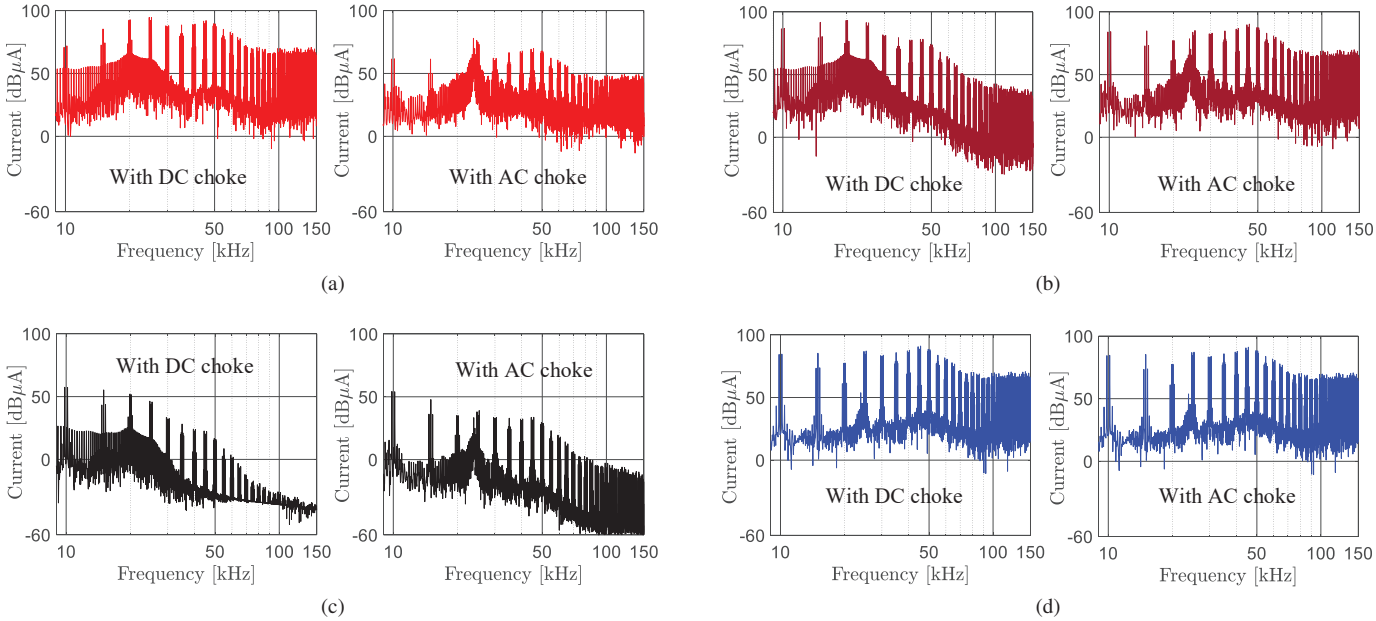

Fig. 7. CM current FFTs of three-phase ASD (see Fig. 2) with DC and AC chokes in the drive (rated power of 7.5 kW). (a) $i_{g-DCLink}$, (b) i_{g-EMI}, (c) i_{LISN}, (d) $i_{g-Motor}$.

[4] P. Waide and C. U. Brunner, "Energy efficiency policy opportunities for electric motor-driven systems," *International Energy Agency (IEA)*, 2011.

[5] F. Zare, H. Soltani, D. Kumar, P. Davari, H. A. M. Delpino, and F. Blaabjerg, "Harmonic emissions of three-phase diode rectifiers in distribution networks," *IEEE Access*, vol. 5, pp. 2819–2833, 2017.

[6] M. H. J. Bollen, P. F. Ribeiro, E. O. A. Larsson, and C. M. Lundmark, "Limits for voltage distortion in the frequency range 2 to 9 kHz," *IEEE Transactions on Power Delivery*, vol. 23, no. 3, pp. 1481–1487, 2008.

[7] J. Barros, R. I. Diego, and M. de Apraíz, "A discussion of new requirements for measurement of harmonic distortion in modern power supply systems," *IEEE Transactions on Instrumentation and Measurement*, vol. 62, no. 8, pp. 2129–2139, 2013.

[8] J. Yaghoobi, A. Abdullah, D. Kumar, F. Zare, and H. Soltani, "Power quality issues of distorted and weak distribution networks in mining industry: A review," *IEEE Access*, vol. 7, pp. 162 500–162 518, 2019.

[9] J. Yaghoobi, F. Zare, T. Rehman, and H. Rathnayake, "Analysis of high frequency harmonics in distribution networks: 9 – 150 kHz," in *2019 IEEE International Conference on Industrial Technology (ICIT)*, 2019, pp. 1229–1234.

[10] B. John, A. Ghosh, and F. Zare, "Investigation on filter requirements and stability effects of sic mosfet-based high-frequency grid-connected converters," *The Journal of Engineering*, vol. 2019, no. 17, pp. 4331–4335, 2019.

[11] P. Kotsampopoulos, A. Rigas, J. Kirchhof, G. Messinis, A. Dimeas, N. Hatziargyriou, V. Rogakos, and K. Andreadis, "EMC issues in the interaction between smart meters and power-electronic interfaces," *IEEE Transactions on Power Delivery*, vol. 32, no. 2, pp. 822–831, 2017.

[12] S. Sakar, S. Rönnberg, and M. Bollen, "Interferences in ac–dc led drivers exposed to voltage disturbances in the frequency range 2–150 kHz," *IEEE Transactions on Power Electronics*, vol. 34, no. 11, pp. 11 171–11 181, 2019.

[13] M. M. AlyanNezhadi, H. Hassanpour, and F. Zare, "Grid-impedance estimation in high-frequency range with a single signal injection using time–frequency distribution," *IET Science, Measurement Technology*, vol. 13, no. 7, pp. 1009–1018, 2019.

[14] K. G. Khajeh, D. Solatialkaran, F. Zare, and N. Mithulananthan, "Harmonic analysis of multi-parallel grid- connected inverters in distribution networks: Emission and immunity issues in the frequency range of 0-150 kHz," *IEEE Access*, vol. 8, pp. 56 379–56 402, 2020.

[15] A. Ganjavi, H. Rathnayake, F. Zare, D. Kumar, J. Yaghoobi, P. Davari, and A. Abbosh, "Common-mode current prediction and analysis in motor drive systems for the new frequency range of 2–150 kHz," *IEEE Journal of Emerging and Selected Topics in Power Electronics*, pp. 1–1, 2020.

[16] A. Ganjavi, H. Rathnayake, F. Zare, D. Kumar, A. Abbosh, and P. Davari, "Investigating the effect of different parameters on harmonics and EMI emissions at the frequency range of 0–9 kHz," in *2020 22nd European Conference on Power Electronics and Applications (EPE'20 ECCE Europe)*, 2020, pp. P.1–P.10.

[17] H. Rathnayake, A. Ganjavi, F. Zare, D. Kumar, and P. Davari, "Common-mode noise modelling and resonant estimation in a three-phase motor drive system: 9-150 kHz frequency range," in *2020 22nd European Conference on Power Electronics and Applications (EPE'20 ECCE Europe)*, 2020, pp. 1–10.